Species-specific pathogenicity of severe fever with thrombocytopenia syndrome virus is determined by anti-STAT2 activity of NSs

Rokusuke Yoshikawa[1,2§], Saori Sakabe[1,3§], Shuzo Urata[1,2], and Jiro Yasuda[1,2,3*]

[1]Department of Emerging Infectious Diseases, Institute of Tropical Medicine (NEKKEN), [2]National Research Center for the Control and Prevention of Infectious Diseases (CCPID), [3]Graduate School of Biomedical Sciences and Program for Nurturing Global Leaders in Tropical and Emerging Communicable Diseases, Nagasaki University, 1-12-4 Sakamoto, Nagasaki 852-8523, Japan.

[§]Equal contributions

*Corresponding author: Jiro Yasuda

Department of Emerging Infectious Diseases, Institute of Tropical Medicine (NEKKEN), Nagasaki University, 1-12-4 Sakamoto, Nagasaki 852-8523, Nagasaki, Japan.

Phone: +81-95-819-7848, FAX: +81-95-819-7848, E-mail: j-yasuda@nagasaki-u.ac.jp

19 Running title: Species-specific pathogenicity of SFTSV

20

ABSTRACT

Severe fever with thrombocytopenia syndrome virus (SFTSV) is a novel emerging virus that has been identified in China, South Korea, and Japan, and induces thrombocytopenia and leukocytopenia in humans with a high case fatality rate. SFTSV is pathogenic to humans, while immunocompetent adult mice and golden Syrian hamsters infected with SFTSV never show apparent symptoms. However, mice deficient for the gene encoding the α chain of the interferon (IFN) α and β receptor (*Ifnar1*$^{-/-}$ mice) and golden Syrian hamsters deficient for the gene encoding signal transducer and activator of transcription 2 (*Stat2*$^{-/-}$ hamsters) are highly susceptible to SFTSV infection, with infection resulting in death. The nonstructural protein (NSs) of SFTSV has been reported to inhibit the type I IFN response through sequestration of human STAT proteins. Here, we demonstrated that SFTSV induces lethal acute disease in STAT2-deficient mice, but not in STAT1-deficient mice. Furthermore, we discovered that NSs cannot inhibit type I IFN signaling in murine cells due to an inability to bind to murine STAT2. Taken together, our results imply that the dysfunction of NSs in antagonizing murine STAT2 can lead to inefficient replication and the loss of pathogenesis of SFTSV in mice.

IMPORTANCE

Severe fever with thrombocytopenia syndrome (SFTS) is an emerging infectious disease caused by SFTS virus (SFTSV), which has been reported in China, South Korea, and Japan. Here, we revealed that mice lacking STAT2, which is an important factor for antiviral innate immunity, are highly susceptible to SFTSV infection. We also show that SFTSV NSs cannot exert its anti-innate immunity activity in mice due to the inability of the protein to bind to murine STAT2. Our findings suggest that the dysfunction of SFTSV NSs as an IFN antagonist in murine cells confers a loss of pathogenicity of SFTSV in mice.

KEYWORDS: SFTSV, NSs, animal model, mouse, STAT2

INTRODUCTION

Severe fever with thrombocytopenia syndrome (SFTS) is an emerging infectious disease caused by the SFTS virus (SFTSV), which is a novel *Phlebovirus* of the *Phenuiviridae* family. SFTSV was first isolated in rural areas of central China in 2011 and subsequently identified in South Korea and Japan (1-4). Moreover, another emerging phlebovirus genetically close to SFTSV, Hartland virus, was found in the United States (5). SFTS is clinically characterized by fever, vomiting, diarrhea, thrombocytopenia, leukocytopenia, and elevated serum levels of enzymes, such as creatine kinase (CK), aspartate aminotransferase (AST), alanine transaminase (ALT), and lactate dehydrogenase (LDH) (6-8). However, the pathogenesis of SFTSV in humans is still poorly understood, and no effective vaccines or antiviral drugs are currently available for treatment of SFTS.

The SFTSV genome is composed of three negative-strand RNA segments (S, M, and L). The L segment encodes the viral RNA-dependent RNA polymerase (L), the M segment encodes the glycoprotein precursors (Gn and Gc), and the S segment encodes the nucleocapsid protein (N) and nonstructural protein (NSs).

The innate immune response, including the type I interferon (IFN) response, is important for preventing viral infection (9). Antiviral innate immunity is initiated by the

recognition of viral infection through cellular pattern recognition receptors (PRRs), such as transmembrane toll-like receptor 3 (TLR3), cytosolic RIG-I-like receptors, and MDA5 (10). Upon recognition, this signal cascade leads to the induction of type I IFN. The activation of the IFN signaling pathway by the binding of secreted IFN to IFN receptors results in the phosphorylation of STAT1 and STAT2. The heterodimer or homodimer of phosphorylated STAT forms heterotrimeric interferon-stimulated gene factor 3 (ISGF3) with IRF-9. The translocation of ISGF3 into the cell nucleus results in the activation of antiviral IFN-stimulated genes (ISGs) by its binding to an IFN-stimulated response element (ISRE) (11). However, during a phlebovirus infection, viral NSs is thought to play a major role in repressing the innate immune response by targeting the IFN response pathway as an IFN antagonist (12-15). Previous studies have reported that NSs of SFTSV inhibits type I and III IFN responses through sequestration of human STAT2 protein in viral replication complexes (13-15).

SFTSV infections do not cause severe disease in immunocompetent mice and golden Syrian hamsters, while type I IFN receptor knock-out (*Ifnar1*$^{-/-}$) mice, which lack the gene encoding the α chain of the IFN α and β receptor, and STAT2-deficient golden Syrian hamsters are highly susceptible to SFTSV, with infection resulting in death (16-19). This suggests that efficient replication of SFTSV in mice and hamsters is

prevented by antiviral innate immunity and that NSs of SFTSV does not inhibit IFN signaling in murine and hamster cells. STAT1 and STAT2 are important factors for antiviral innate immunity. However, the relationship between SFTSV pathogenicity and STAT function remains unknown. In this study, to investigate the role of STAT1 and STAT2 in the pathogenesis and replication of SFTSV in mice, we examined the pathogenicity of SFTSV in *Stat1*$^{-/-}$ and *Stat2*$^{-/-}$ mice and measured the antagonistic activities of NSs against IFN signaling in murine cells.

RESULTS

SFTSV infection to *Ifnar1*$^{-/-}$ mice.

It has been reported that *Ifnar1*$^{-/-}$ mice are highly susceptible to SFTSV strains YL-1 and SPL010, with infection resulting in death (16-17). In this study, we used the YG-1 strain isolated from the first SFTS patient reported in Japan (4). Wild-type C57BL/6 mice and *Ifnar1*$^{-/-}$ mice were intradermally (id) inoculated with 10 focus forming units (FFU) of the SFTSV (YG-1). All infected wild-type mice survived without any clinical signs (Fig. 1A). In contrast, all infected *Ifnar1*$^{-/-}$ mice died 5 to 8 days after infection (Fig. 1A). Moreover, all *Ifnar1*$^{-/-}$ mice infected with SFTSV showed severe body weight loss, leukocytopenia, and thrombocytopenia 1–7 days postinfection (pi) (Fig. 1B–D). The titers of SFTSV in the organs (brains, lungs, livers, spleens, kidneys, and intestines) and plasma of infected *Ifnar1*$^{-/-}$ and wild-type mice were also measured by focus forming assay at 3, 5, and 7 days pi. As shown in Fig. 2, efficient viral replication in *Ifnar1*$^{-/-}$ mice was observed in the spleen and plasma at 3 days pi, all organs at 5 days pi, and the spleen, kidney, and intestine at 7 days pi. In contrast, we could not detect infectious SFTSV in the plasma or organs of wild-type mice.

The results show that the SFTSV (YG-1) induces lethal acute infection accompanied by thrombocytopenia in *Ifnar1*$^{-/-}$ mice.

SFTSV causes lethal infection in *Stat2*$^{-/-}$ mice, but not *Stat1*$^{-/-}$ mice.

Next, to investigate the roles of STAT1 and STAT2 in SFTSV infection, *Stat1*$^{-/-}$, *Stat2*$^{-/-}$, and *Ifnar1*$^{-/-}$ mice were infected with YG-1 strain. None of the infected *Stat2*-/- mice survived, while all of the *Stat1*$^{-/-}$ mice infected with YG-1 survived (Fig. 1A). As shown in Fig. 1B, *Stat2*$^{-/-}$ mice lost body weight at 1–7 days pi, while *Stat1*$^{-/-}$ mice lost body weight at 1-5 days pi, and then recovered. Unlike in *Ifnar1*$^{-/-}$ mice, the number of white blood cells in *Stat1*$^{-/-}$ and *Stat2*$^{-/-}$ mice transiently decreased after infection and then recovered to normal values (Fig. 1C). Both *Stat1*$^{-/-}$ and *Stat2*$^{-/-}$ mice infected with SFTSV showed thrombocytopenia regardless of survival (Fig. 1D). This implies that the lethality of SFTSV is not associated with thrombocytopenia. Next, we measured the titers of SFTSV in organs (brains, lungs, livers, spleens, kidneys, and intestines) and plasma of infected *Stat1*$^{-/-}$ and *Stat2*$^{-/-}$ mice by focus forming assay at 3, 5, and 7 days pi. In *Stat2*$^{-/-}$ mice, SFTSV was detected in the plasma, spleen, and kidney at 3 days pi, the plasma and all organs at 5 days pi, and the spleen and kidney at 7 days pi. In *Stat1*$^{-/-}$ mice, SFTSV replicated in the lung, spleen, kidney, intestine, and plasma; however, the maximum titers of SFTSV in these organs and plasma were lower than those in *Stat2*$^{-/-}$ mice (Fig. 2).

These results indicate that *Stat2*$^{-/-}$ and *Ifnar1*$^{-/-}$ mice, but not *Stat1*$^{-/-}$ mice, are highly susceptible to SFTSV infection, which suggests that STAT2 plays a critical role in the suppression of SFTSV replication in mice.

SFTSV NSs cannot suppress type I IFN signaling in murine cells.

It has been reported that SFTSV suppress type I IFN signaling in human cells (13). Therefore, we hypothesized that SFTSV cannot suppress type I IFN signaling in murine cells, and IFN-mediated innate immunity restricts SFTSV replication in mice. To address this possibility, the ISRE activation by SFTSV infection was examined in human-derived HEK293T cells and mouse-derived NIH3T3 cells using dual-luciferase reporter (DLR) gene assay. As shown in Fig 3A, SFTSV infection did not induce the ISRE activation in HEK293T cells, while the ISRE activation was induced by SFTSV infection in NIH3T3 cells. These results suggest that SFTSV cannot inhibit type I IFN signaling in murine cells.

Recently, SFTSV NSs has been reported to function as an IFN antagonist (13-15)., Therefore, the effects of NSs on ISRE activation in HEK293T cells and NIH3T3 cells were examined by DLR gene assay. In this experiment, the VP40 protein of mouse-adapted Marburg virus (mMARV), which functions as an IFN signaling inhibitor

149 in murine cells, was used as a positive control (20). As shown in Fig. 3B, IFN-αA/D
150 treatment induced strong ISRE activation in both HEK293T and NIH3T3 cells. As
151 expected, the expression of SFTSV NSs significantly inhibited the ISRE activation
152 driven by IFN-αA/D in HEK293T cells, while NSs expression did not suppress this
153 activation in NIH3T3 cells (Fig. 3B). We also confirmed that the ISRE activation driven
154 by IFN-αA/D in NIH3T3 cells was suppressed by the expression of mMARV VP40 (Fig.
155 3C). These results suggest that SFTSV NSs cannot interfere with type I IFN signaling in
156 murine cells.

157 We also examined the effect of NSs on IFN-αA/D-induced expression of mRNA
158 for two ISGs, ISG56 and oligoadenylate synthetase 1 (OAS1), by real-time qPCR. The
159 induction of both ISGs by IFN in HEK293T cells was suppressed by NSs expression,
160 whereas NSs did not suppress induction in NIH3T3 cells (Fig. 3D).

161

162 **NSs does not interact with murine and hamster STAT2.**

163 SFTSV NSs inhibits type I IFN signaling by the interaction with human STAT1
164 (hSTAT1) and STAT2 (hSTAT2) (13-15). However, the interaction with hSTAT1 is
165 weaker than that with hSTAT2 (15). We also showed here that mice deficient for STAT2,
166 but not STAT1, were highly susceptible to SFTSV infection and progressed to severe

167 disease (Fig1). Therefore, we suggest that NSs cannot interact with murine STAT2 and
168 thus cannot antagonize IFN signaling in murine cells.

169 First, to examine whether NSs interacts with murine STAT2 (mSTAT2), we
170 performed co-immunoprecipitation (co-IP) assays using lysates from cells transfected
171 with a NSs expression plasmid. As shown in Fig. 4A, co-IP of STAT2 with NSs was
172 observed only in the lysates from HEK293T cells, but not from NIH3T3 cells,
173 suggesting that NSs interact with hSTAT2 but not with mSTAT2. It was also indicated
174 that NSs bound to hSTAT1, but not to murine STAT1 (mSTAT1) (Fig. 4A).

175 We also examined the interaction of NSs with hamster STAT2 (hamSTAT2) by
176 co-IP assay, since *Stat2*$^{-/-}$ hamsters, like S*tat2*$^{-/-}$ mice, are highly susceptible to SFTSV
177 infection (19). As shown in Fig. 4B, the interaction of NSs with hamSTAT2, as well as
178 mSTAT2, was not observed.

179 The interaction of NSs with STAT2 was also examined by subcellular
180 colocalization of the proteins. The NSs expression plasmid was cotransfected with the
181 expression plasmids for hSTAT2, mSTAT2, or hamSTAT2 into HEK293T, NIH3T3, or
182 BHK-21 cells, respectively, and subcellular localizations of proteins were observed.
183 Cytoplasmic inclusion bodies (IBs), mainly formed by NSs, were also observed in
184 HEK293T, NIH3T3, and BHK-21 cells (Fig. 4C). In HEK293T cells, hSTAT2

colocalizes with NSs, consistent with previous reports (13-15). On the other hand, in NIH3T3 and BHK-21 cells, colocalization of NSs with mSTAT2 or hamSTAT2 was not observed (Fig. 4C). These findings indicate that NSs interacts with hSTAT2, but not mSTAT2 and hamSTAT2.

The N-terminal region of hSTAT2 is important for binding to NSs.

To investigate the difference in NSs binding between human and murine STAT2, we prepared a series of chimeric proteins from hSTAT2 and mSTAT2 (Fig. 5A). The interactions between NSs and the chimeric STAT2 proteins were examined by co-IP assay. All chimeric proteins efficiently expressed in NIH3T3 cells (Fig. 5B). As shown in Fig. 5B, NSs interacted with hSTAT2, HHM, HMM, H(101–315)MM, and H(101–315)HM, but not mSTAT2, MHH, MMH, H(1–100)MM, H(1–221)MM and H(222–315)MM.

We also confirmed the results by observation of colocalization of the proteins (Fig. 5C). NSs colocalized with hSTAT2, HHM, HMM, H(101–315)MM and H(101–315)HM, while mSTAT2, MHH, MMH, H(1–100)MM, H(1–221)MM, and H(222–315)MM, did not colocalize with NSs. These results are consistent with those from the co-IP assay. It has been reported that SFTSV NSs interacts with the DNA-binding

domain (DBD: amino acid position 316–485) of hSTAT2 (13). Taken together, these results suggest that region 101–315 of hSTAT2 is important for the binding to NSs in addition to the DBD, or that this region of mSTAT2 interferes with the binding to NSs.

To further examine whether MHH and MMH, which cannot bind to NSs, function as STAT2 proteins in the presence of NSs, ISRE activation by MHH or MMH in the presence of NSs was investigated by the DLR assay in HEK293T cells. ISRE activation was reduced by NSs in the absence of exogenous STAT2, and overexpression of exogenous hSTAT2 slightly compensated for this reduction induced by NSs (Fig. 6). In contrast, the suppression of ISRE activation by NSs was significantly recovered by mSTAT2, MMH, and MHH, suggesting that MMH and MHH, as well as mSTAT2, activate ISRE as a functional STAT2 protein in the presence of NSs in HEK293T cells.

Type I IFN induces the phosphorylation of mSTAT2 in the presence of NSs.

Tyrosine phosphorylation of STAT2 is important for its function as a transcription factor in the type I IFN signaling pathway (21). To assess whether type I IFN signaling can phosphorylate mSTAT2 in the presence of NSs, HEK293T and NIH3T3 cells were transfected with empty vector or the NSs-HA expression plasmid, and then treated with IFN-αA/D. The expression levels of hSTAT2 and mSTAT2 were stable regardless of

NSs expression (Fig. 7A). In the absence of NSs, IFN induced the phosphorylation of hSTAT2 and mSTAT2. hSTAT2 phosphorylation in HEK293T cells was significantly downregulated by NSs in a concentration-dependent manner. In contrast, mSTAT2 in NIH3T3 cells was phosphorylated irrespective of NSs expression (Fig. 7A). These were also observed in SFTSV infected cells (Fig. 7B). It is likely that NSs cannot interfere with the phosphorylation of mSTAT2, since NSs cannot bind to mSTAT2.

DISCUSSION

Previous studies in animal models of SFTSV infection indicated the importance of the type I IFN response in mice and STAT2 in hamsters to prevent disease progression (16-17, 19). Both STAT1 and STAT2 have been found to be key factors in the IFN signaling pathway (21). In this study, we demonstrated that STAT2-deficient mice, as well as type I IFN receptor-deficient mice, are more susceptible to SFTSV than STAT1-deficient mice and wild-type mice. Moreover, our results indicate that NSs has no ability to suppress the IFN signaling pathway in murine cells because NSs, which binds hSTAT1 and hSTAT2, cannot interact with mSTAT1 and mSTAT2. The SFTSV growth in the organs of *Stat1*$^{-/-}$ mice were much less efficient than those in *Stat2*$^{-/-}$ and *Ifnar1*$^{-/-}$ mice, although SFTSV could grow in *Stat1*$^{-/-}$ mice (Fig. 2). In addition, SFTSV infection induced milder symptom in *Stat1*$^{-/-}$ mice than in *Stat2*$^{-/-}$ and *Ifnar1*$^{-/-}$ mice (Fig. 1). These suggests that innate immunity dependent on STAT2, but not STAT1, strongly inhibits the replication of SFTSV in mice. In several human cell lines, the expression of some ISGs is upregulated by STAT2, independent of STAT1 (22). For example, the expression levels of several ISGs including APOBEC3G, PKR, ISG15, and Mx1 are increased by type I IFN stimulation regardless of STAT1 expression in the human liver cell lines, Huh7 and Hep3B. However, when the expression of STAT2 is suppressed, the

246 expression levels of these ISGs are not increased after type I IFN treatment. These
247 findings suggest that ISGs expression mediated by STAT2, but not STAT1, suppress
248 mainly SFTSV infection in mice.

249 SFTSV causes severe disease in human, while immunocompetent adult mice
250 never show any apparent severe symptoms after SFTSV infection (18). In this study, we
251 showed that mice lacking STAT2 are highly susceptible to SFTSV infection. Moreover,
252 NSs can suppress the phosphorylation of hSTAT2, whereas the phosphorylation of
253 mSTAT2 is not inhibited by NSs due to the inability of NSs to bind to mSTAT2. The
254 data also indicates that NSs cannot interact with hamSTAT2. This result is consistent
255 with a previous report showed that STAT2-deficient hamsters are also highly susceptible
256 to SFTSV infection (19).

257 The relationship between NSs and STAT2 is reminiscent of that of dengue virus
258 NS5 and STAT2 (A23-25). Previous studies reported that innate immunity mediated by
259 mSTAT2 restricts dengue virus replication in mice (25-26). To block the type I IFN
260 signaling pathway in humans, dengue virus NS5 expression leads to the degradation of
261 hSTAT2 (25). However, NS5 cannot suppress type I IFN signaling in mice, because
262 mSTAT2 is resistance to NS5-mediated degradation (23-25). These results demonstrate
263 that STAT2 may be one of the determinants for the species specificity of dengue virus.

Here, we elucidated that SFTSV induces lethal disease in STAT2-deficient mice and that NSs cannot interact with mSTAT2. Thus, similar to dengue virus NS5, the anti-STAT2 activity of NSs appears to determine the species specificity of SFTSV infection.

In this study, chimeric mutants of hSTAT2 and mSTAT2 revealed that residues 101–315 of hSTAT2 are required for the interaction with NSs or that these residues in mSTAT2 interfere with the interaction with NSs. We also confirmed that mSTAT2 and all of the chimeric mutants of hSTAT2 and mSTAT2 used in this study can activate ISRE-mediated gene expression as functional STAT2 proteins. Previously, Ning *et al.* reported that the DBD region (316–485) of hSTAT2 is required for the interaction with NSs (13). However, we showed that mutants possessing the DBD region of mSTAT2, HMM, and H(101–315)MM, can still bind to NSs (Fig. 5). At present, we cannot explain this result, although this discrepancy may be explained by the differences in the three-dimensional protein structure between our mutants and Ning's deletion mutants. Further analyses will be required to clarify this issue.

Taken together, we conclude that the anti-STAT2 activity of NSs determines the species specificity of SFTSV infection. In addition, we show that *Stat2*$^{-/-}$ mice, as well as *Ifnar1*$^{-/-}$ mice and *Stat2*$^{-/-}$ hamsters, are highly susceptible to SFTSV infection, which causes lethal disease, suggesting that *Stat2*$^{-/-}$ mice may be useful as an animal model to

282 develop antiviral drugs against SFTSV infection.

283

MATERIALS AND METHODS

Ethics statement.

Our research protocol for the use of mice follows the Nagasaki University Regulations for Animal Care and Use, which was approved by the Animal Experiment Committee of Nagasaki University (approval number; 151110-1-5).

Animals.

B6.129-Dnase2a<tm10sa>Ifnar1<tm1Agt> mouse strain (RBRC04021; *Ifnar1*$^{-/-}$ *Dnase2a*$^{+/-}$) (27) was provided by RIKEN BRC through the National BioResource Project of MEXT, Japan. *Ifnar1*$^{-/-}$ mice were generated by crossing *Dnase2a*$^{+/-}$ *Ifnar1*$^{-/-}$ parents. *Stat1*$^{-/-}$ mice were provided by Dr. Takayuki Yoshimoto (Tokyo Medical University). *Stat2*$^{-/-}$ mice were purchased from the Jackson Laboratory. The genetical backgrounds of all mice used in this study are C57BL/6.

SFTSV infection in mice.

Six- to eight-week-old male or female mice were used in this study. In infection experiments, each mouse was infected with SFTSV by intradermal injection (50 μL of virus solution for 10 FFU). Mouse survival and body weight changes were monitored

daily for 14 days pi. At 1, 3, and 7 days pi, blood was collected, and platelets and leukocytes were counted using a hematology analyzer (Sysmex pocH-100iV; Sysmex or VetScan HMII; Abaxis). Mice were euthanized, and plasma and organs (lungs, livers, spleens, kidneys, intestines, and brains) were collected. Viruses in plasma were titrated by focus forming assay using Vero E6 cells. To determine the titer of SFTSV in organs, mouse organs were collected in a 9-fold volume of minimum essential media (Sigma-Aldrich) and then disrupted through high-speed shaking using TissueLyser II (Qiagen). After centrifugation (700 x g, 5min, 4°C), the amounts of viruses in the homogenates (10% w/v) were determined by focus forming assay in VeroE6 cells. The limit of detection is 100FFU/g.

Cell culture and virus.

Human embryonic kidney (HEK) 293T (CRL-11268; ATCC), NIH3T3 (CRL-1658; ATCC), BHK-21 (JCRB9020; Health Science Research Resources Bank (HSRRB)), and Vero E6 (CRL-1586; ATCC) cells were cultured in Dulbecco modified Eagle medium (Sigma-Aldrich) supplemented with 10% heat-inactivated (fetal calf serum) FCS and antibiotics (Thermo Fisher Scientific). The SFTSV (YG1), a field isolate from an SFTS patient in Japan, was kindly provided by Dr. Ken Maeda, Yamaguchi

University (28). The virus stocks were prepared from culture supernatants of Vero E6 cells.

Focus forming assay.

SFTSV titers were determined using a focus forming assay. Briefly, confluent monolayers of Vero E6 cells were inoculated with 10-fold dilutions of SFTSV and incubated at 37°C for 1 hour. The inoculum was removed, and cells were washed and overlaid with MEM (Sigma-Aldrich) containing 0.7% agarose and 0.7% FCS. After 4 days, cells were fixed with 4% paraformaldehyde and permeabilized with phosphate-buffered saline (PBS) containing 1% Triton X-100. Cells were blocked with PBS containing 0.1% Triton X-100 and 1% bovine serum albumin (BSA), and then incubated with anti-SFTSV N protein rabbit polyclonal antibody (28). After washing with PBS, the cells were incubated with anti-rabbit IgG conjugated with horseradish peroxidase (Promega). After more washes with PBS, SFTSV-infected cells were detected by using Peroxidase Stain DAB Kit and Metal Enhancer for DAB Stain (Nacalai Tesque). The number of SFTSV N positive cells were determined and normalized as FFU/ml.

Plasmids.

The open reading frame (ORF) encoding NSs was amplified by reverse transcription PCR (RT-PCR) from SFTSV (YG-1) viral RNA and inserted into pcDNA3.1 (Invitrogen) with a hemagglutinin (HA) tag using the primers listed in Table 1 to produce pcDNA3.1/NSs-HA. To prepare the expression plasmids for 6xHistidine (His)-tagged hSTAT2 (pcDNA3.1/hSTAT2-His), mSTAT2 (pcDNA3.1/mSTAT2-His), and hamSTAT2 (pcDNA3.1/hamSTAT2-His), the desired genes were amplified by RT-PCR using the primers listed in Table 1 from the cDNA of HEK293T, NIH3T3, and BHK-21 cells, respectively. The expression plasmids for the series of STAT2 chimeras were constructed using an In-Fusion HD Cloning kit (TaKaRa) with the primers listed in Table 1. The expression plasmid for mMARV VP40 was constructed from MARV VP40 (28) using a KOD-Plus-Mutagenesis Kit (TOYOBO) using the primers listed in Table 1.

Reporter gene assay.

HEK293T cells and NIH3T3 cells were cotransfected with ISRE reporter plasmid (450 ng) (Promega) and pRL-TK plasmid [the *Renilla* luciferase control plasmid for the constitutively active herpes simplex virus (HSV)-thymidine kinase (TK) promoter] (100

ng) (Promega). Twenty-four hours after transfection, the transfected cells were mock-infected or infected with SFTSV. Two days after infection, luciferase activities were measured with a DLR assay kit (Promega) and a TriStar LB941 system (Berthold). For the reporter gene assays with SFTSV NSs transfection, the ISRE reporter plasmid (500 ng) (Promega) and pRL-TK [the *Renilla* luciferase control plasmid for the constitutively active herpes simplex virus (HSV)-thymidine kinase (TK) promoter] plasmid (100 ng) (Promega) were transfected into HEK293T and NIH3T3 cells with or without the indicated amount of pcDNA3.1/NSs-HA plasmid or the expression plasmid for mMARV VP40 (800 ng) using LT-1 (Mirus) or Lipofectamine 3000 (Thermo Fisher Scientific) according to the manufacturer's instructions. Twenty-four hours after transfection, cells were treated with IFN-αA/D (500 U/ml) (Sigma-Aldrich) or were left untreated for 18 h. Luciferase activities then were measured with a DLR assay kit (Promega) and a TriStar LB941 system (Berthold).

Quantitative real-time reverse transcription PCR (RT-PCR) of IFN-treated cells.

Total RNA was extracted from HEK293T and NIH3T3 cells using an RNeasy Mini kit (Qiagen). Real-time RT-PCR was performed by using the One Step TB Green™ PrimeScript™ PLUS RT-PCR Kit (TaKaRa) according to the manufacturer's

instructions, and the PCR primers used in this study are listed in Table 1. Relative mRNA levels were calculated by the $2^{-\Delta\Delta CT}$ method with *GAPDH* mRNA as an internal control and are shown as relative fold changes normalized to the untreated control samples.

Immunoblotting.

Protein samples were separated by SDS-PAGE and transferred to nitrocellulose membranes (Millipore). After blocking with 5% skim milk in Tris-buffered saline/Tween 20 (TBS-T), the membranes were incubated with each of the following antibodies: anti-HA (18850; QED Biosciences Inc.), anti-His (9F2; Wako), anti-hSTAT2 (A-9; Santa Cruz), anti-mSTAT2 (07-140; Merc), anti-STAT2 (phosphor Y690) (ab53132; Abcam), anti-STAT1 (D19KY; Cell signaling) or anti-β actin (AC-15; Sigma-Aldrich). After washing with TBS-T, the membranes were incubated with horseradish peroxidase-labeled secondary antibodies, Anti-Mouse IgG-HRP (A2304; Sigma-Aldrich) or Anti-Rabbit IgG-HRP (WA4011; Promega), and then detected using ECL prime (GE Healthcare) according to the manufacturer's instructions. Bands were visualized using an image analyzer (LAS-4000 mini; GE Healthcare).

Co-IP assay.

To examine the binding of NSs to endogenous STAT2, the pcDNA3.1/NSs-HA plasmid (15 μg) was transfected into HEK293T and NIH3T3 cells in 10-cm dishes (Thermo Fisher Scientific) using LT-1 or Lipofectamine 3000, respectively. To examine the binding of NSs to exogenous STAT2 or STAT2 derivatives, the pcDNA3.1/NSs-HA plasmid (3 μg) was cotransfected into NIH3T3 cells with each STAT2 expression plasmid (1 μg) in 6-well plates (Thermo Fisher Scientific) using Lipofectamine 3000. Two days after transfection, cells were lysed in lysis buffer (25 mM Tris-HCl, 150 mM NaCl, 1 mM EDTA, and 1% Triton X-100) containing a protease inhibitor cocktail (Roche). To perform the co-IP assay, cell lysates were mixed with magnetic beads conjugated to an anti-His monoclonal antibody (OGHis; MBL) or anti-HA monoclonal antibody (5D8; MBL) and incubated at 4°C for 3 h or overnight, respectively. Then, the magnetic beads were washed with lysis buffer and wash buffer (50 mM Tris-HCl, 1% NP-40, 0.25% deoxycholic acid sodium salt, 150 mM NaCl, and 1 mM EDTA) and analyzed by immunoblotting as described above.

Immunofluorescence assay (IFA).

The expression plasmids for His-tagged hSTAT2, mSTAT2, hamSTAT2, or a series of

STAT2 chimeras were cotransfected into HEK293T, NIH3T3, or BHK-21 cells with the pcDNA3.1/NSs-HA plasmid. Twenty-four hours after transfection, transfected cells were fixed using 4% paraformaldehyde-PBS (Wako), and then the fixed cells were incubated in 1% Triton X-100 in PBS for permeabilization and blocked in 10% FCS in blocking buffer (3% BSA and 0.3% Triton X-100 in PBS). Cells then were treated with primary antibodies (anti-HA (18850; QED Biosciences Inc.) or anti-His (9F2; Wako)) overnight at 4°C and stained with secondary antibodies (Anti-Rabbit IgG - H&L (FITC) (ab6009; abcam) or Anti-Mouse IgG (whole molecule) −TRITC (T5393; Sigma-Aldrich)) for 2 h at room temperature with DAPI (Roche) for visualization of nuclei. Image acquisition was performed with a LSM780 microscope (Carl Zeiss)

Statistical analyses. Significant differences in virus titers in mouse organs among mouse strains were determined by one-way ANOVA following Tukey's multiple comparisons test using GraphPad Prism software. And statistically significant differences in the data of Fig3A, 3B, 3C, 3D and 6 were determined using Student's *t*-test (Fig3A. 3C and 3D) or Dunnett's test (Fig 3B and 6).

ACKNOWLEDGMENTS

We would like to thank Dr. K. Maeda (Yamaguchi University, Yamaguchi, Japan) and Dr. T. Yoshimoto (Tokyo Medical University, Tokyo, Japan) for providing the SFTSV YG1 strain and *Stat1*$^{-/-}$ mice, respectively. We also would like to thank Dr. S. Morikawa and Dr. S. Fukushi (National Institute of Infectious Diseases, Tokyo, Japan) for providing the anti-SFTSV N antibody. We are grateful to all the members of the Department of Emerging Infectious Diseases, Institute of Tropical Medicine, Nagasaki University. This research was supported by a grant from the Japan Agency for Medical Research and Development (AMED) under Grant Number JP18fk0108202h0805 (JY), the Japan Society for the Promotion of Science under Grant Number 15J06242 (RY), and the Takeda Science Foundation (RY).

REFERENCES

1 Yu XJ, Liang MF, Zhang SY, Liu Y, Li JD, Sun YL, Zhang L, Zhang QF, Popov VL, Li C, Qu J, Li Q, Zhang YP, Hai R, Wu W, Wang Q, Zhan FX, Wang XJ, Kan B, Wang SW, Wan KL, Jing HQ, Lu JX, Yin WW, Zhou H, Guan XH, Liu JF, Bi ZQ, Liu GH, Ren J, Wang H, Zhao Z, Song JD, He JR, Wan T, Zhang JS, Fu XP, Sun LN, Dong XP, Feng ZJ, Yang WZ, Hong T, Zhang Y, Walker DH, Wang Y, Li DX. 2011. Fever with thrombocytopenia associated with a novel bunyavirus in China. N Engl J Med 364:1523-1532.

2 Denic S, Janbeih J, Nair S, Conca W, Tariq WU, Al-Salam S. 2011. Acute thrombocytopenia, leucopenia, and multiorgan dysfunction: the first case of SFTS bunyavirus outside China? Case Rep Infect Dis: 204056.

3 Kim KH, Yi J, Kim G, Choi SJ, Jun KI, Kim NH, Choe PG, Kim NJ, Lee JK, Oh MD. 2013. Severe fever with thrombocytopenia syndrome, South Korea, 2012. Emerg Infect Dis 19:1892-1894.

4 Takahashi T, Maeda K, Suzuki T, Ishido A, Shigeoka T, Tominaga T, Kamei T, Honda M, Ninomiya D, Sakai T, Senba T, Kaneyuki S, Sakaguchi S, Satoh A, Hosokawa T, Kawabe Y, Kurihara S, Izumikawa K, Kohno S, Azuma T, Suemori K, Yasukawa M, Mizutani T, Omatsu T, Katayama Y, Miyahara M, Ijuin M, Doi K,

457 Okuda M, Umeki K, Saito T, Fukushima K, Nakajima K, Yoshikawa T, Tani H,
458 Fukushi S, Fukuma A, Ogata M, Shimojima M, Nakajima N, Nagata N, Katano H,
459 Fukumoto H, Sato Y, Hasegawa H, Yamagishi T, Oishi K, Kurane I, Morikawa S,
460 Saijo M. 2014. The first identification and retrospective study of Severe Fever with
461 Thrombocytopenia Syndrome in Japan. J Infect Dis 209:816-827.
462 5 McMullan LK, Folk SM, Kelly AJ, MacNeil A, Goldsmith CS, Metcalfe MG,
463 Batten BC, Albarino CG, Zaki SR, Rollin PE, Nicholson WL, Nichol ST. 2012. A
464 new phlebovirus associated with severe febrile illness in Missouri. N Engl J Med
465 367:834–841.
466 6 Cui N, Bao XL, Yang ZD, Lu QB, Hu CY, Wang LY, Wang BJ, Wang HY, Liu K,
467 Yuan C, Fan XJ, Wang Z, Zhang L, Zhang XA, Hu LP, Liu W, Cao WC. 2014.
468 Clinical progression and predictors of death in patients with severe fever with
469 thrombocytopenia syndrome in China. J Clin Virol 59:12-17.
470 7 Lu QB, Yang ZD, Wang LY, Qin SL, Cui N, Wang HY, Li H, Liu K, Hu JG, Zhang
471 XA, Liu W, Cao WC. 2015. Discrimination of novel bunyavirus infection using
472 routine laboratory test. Clin Microbiol Infect204:e1-7.
473 8 Cui N, Liu R, Lu QB, Wang LY, Qin SL, Yang ZD, Zhuang L, Liu K, Li H, Zhang
474 XA, Hu JG, Wang JY, Liu W, Cao WC. 2015. Severe fever with thrombocytopenia

475 syndrome bunyavirus-related human encephalitis. J Infect 70:52-59.
476 9 Koyama S, Ishii KJ, Coban C, Akira S. 2008. Innate immune response to viral
477 infection. Cytokine 43:336-341.
478 10 Habjan M, Pichlmair A. 2015. Cytoplasmic sensing of viral nucleic acids. Curr Opin
479 Virol 11:31-37.
480 11 Schneider WM, Chevillotte MD, Rice CM. 2014. Interferon-stimulated genes: a
481 complex web of host defenses. Annu Rev Immnunol 32:513-545.
482 12 Wuerth JD, Weber F. 2016. Phleboviruses and the type I interferon response. Viruses
483 8:E174.
484 13 Ning YJ, Feng K, Min YQ, Cao WC, Wang M, Deng F, Hu Z, Wang H. 2015.
485 Disruption of type I interferon signaling by the nonstructural protein of severe fever
486 with thrombocytopenia syndrome virus via the hijacking of STAT2 and STAT1 into
487 inclusion bodies. J Virol 89:4227-4236.
488 14 Chaudhary V, Zhang S, Yuen KS, Li C, Lui PY, Fung SY, Wang PH, Chan CP, Li D,
489 Kok KH, Liang M, Jin DY. 2015. Suppression of type I and type III IFN signalling
490 by NS of severe fever with thrombocytopenia syndrome virus through inhibition of
491 STAT1 phosphorylation and activation. J Gen Virol 96:3204-3211.
492 15 Rezelj VV, Li P, Chaudhary V, Elliott RM, Jin DY, Brennan B. 2017. Differential

493 Antagonism of Human Innate Immune Responses by Tick-Borne Phlebovirus
494 Nonstructural Proteins. mSphere 28:e00234-17.
495 16 Tani H, Fukuma A, Fukushi S, Taniguchi S, Yoshikawa T, Iwata-Yoshikawa N, Sato
496 Y, Suzuki T, Nagata N, Hasegawa H, Kawai Y, Uda A, Morikawa S, Shimojima M,
497 Watanabe H, Saijo M. 2016. Efficacy of T-705 (favipiravir) in the treatment of
498 infections with lethal severe fever with thrombocytopenia syndrome virus. mSphere
499 1:e00061-15.
500 17 Liu Y, Wu B, Paessler S, Walker DH, Tesh RB, Yu XJ. 2014. The pathogenesis of
501 severe fever with thrombocytopenia syndrome virus infection in alpha/beta
502 interferon knockout mice: insights into the pathologic mechanisms of a new viral
503 hemorrhagic fever. J Virol 88:1781-1786.
504 18 Jin C, Liang M, Ning J, Gu W, Jiang H, Wu W, Zhang F, Li C, Zhang Q, Zhu H,
505 Chen T, Han Y, Zhang W, Zhang S, Wang Q, Sun L, Liu Q, Li J, Wang T, Wei Q,
506 Wang S, Deng Y, Qin C, Li D. 2012. Pathogenesis of emerging severe fever with
507 thrombocytopenia syndrome virus in C57/BL6 mouse model. Proc Natl Acad Sci U
508 S A 109:10053–10058.
509 19 Gowen BB, Westover JB, Miao J, Van Wettere AJ, Rigas JD, Hickerson BT, Jung
510 KH, Li R, Conrad BL, Nielson S, Furuta Y, Wang Z. 2017. Modeling Severe Fever

511 with Thrombocytopenia Syndrome Virus Infection in Golden Syrian Hamsters:
512 Importance of STAT2 in Preventing Disease and Effective Treatment with
513 Favipiravir. J Virol 91:e01942-16.
514 20 Feagins AR, Basler CF. 2015. Amino Acid Residue at Position 79 of Marburg Virus
515 VP40 Confers Interferon Antagonism in Mouse Cells. J infect Dis 2:219-225.
516 21 Ivashkiv LB, Donlin LT. 2014. Regulation of type I interferon responses. Nat Rev
517 Immunol 14:36-49.
518 22 Sarkis PT, Ying S, Xu R, Yu XF. 2006. STAT1-independent cell type-specific
519 regulation of antiviral APOBEC3G by IFN-alpha. J Immunol 177:4530-4540.
520 23 Ashour, J., Laurent-Rolle, M., Shi, P.Y., and Garcia-Sastre, A. 2009. NS5 of dengue
521 virus mediates STAT2 binding and degradation. J. Virol 83:5408-5418.
522 24 Mazzon, M., Jones, M., Davidson, A., Chain, B., and Jacobs, M. 2009. Dengue virus
523 NS5 inhibits interferon-alpha signaling by blocking signal transducer and activator
524 of transcription 2 phosphorylation. J. Infect. Dis 200:1261–1270.
525 25 Ashour J, Morrison J, Laurent-Rolle M, Belicha-Villanueva A, Plumlee CR,
526 Bernal-Rubio D, Williams KL, Harris E, Fernandez-Sesma A, Schindler C,
527 García-Sastre A. 2010. Mouse STAT2 restricts early dengue virus replication. Cell
528 Host Microbe 18:410-421.

529 26 Perry ST, Buck MD, Lada SM, Schindler C, Shresta S. 2011. STAT2 mediates
530 innate immunity to Dengue virus in the absence of STAT1 via the type I interferon
531 receptor. PLoS Pathog 7:e1001297.
532 27 Yoshida H, Okabe Y, Kawane K, Fukuyama H, Nagata S. 2005. Lethal anemia
533 caused by interferon-beta produced in mouse embryos carrying undigested DNA.
534 Nat Immunol 6:49-56.
535 28 Urata S, Uno Y, Kurosaki Y, Yasuda J. 2018. The cholesterol, fatty acid and
536 triglyceride synthesis pathways regulated by site 1 protease (S1P) are required for
537 efficient replication of severe fever with thrombocytopenia syndrome virus.
538 Biochem Biophys Res Commun 503:631-636.
539 29 Urata S, Noda T, Kawaoka Y, Morikawa S, Yokosawa H, Yasuda J. 2007. Interaction
540 of Tsg101 with Marburg virus VP40 depends on the PPPY motif, but not the
541 PT/SAP motif as in the case of Ebola virus, and Tsg101 plays a critical role in the
542 budding of Marburg virus-like particles induced by VP40, NP, and GP. J Virol
543 81:4895-4899.
544 30 Lee KG, Kim SS, Kui L, Voon DC, Mauduit M, Bist P, Bi X, Pereira NA, Liu C,
545 Sukumaran B, Rénia L, Ito Y, Lam KP. 2015. Bruton's tyrosine kinase
546 phosphorylates DDX41 and activates its binding of dsDNA and STING to initiate

type 1 interferon response. Cell Rep 10:1055-1065.

31 Jiang LJ, Zhang NN, Ding F, Li XY, Chen L, Zhang HX, Zhang W, Chen SJ, Wang ZG, Li JM, Chen Z, Zhu J. 2011. RA-inducible gene-I induction augments STAT1 activation to inhibit leukemia cell proliferation. Proc Natl Acad Sci U S A 108:1897-1902.

32 Cool J, DeFalco TJ, Capel B. 2011. Vascular-mesenchymal cross-talk through Vegf and Pdgf drives organ patterning. Proc Natl Acad Sci U S A 108:167-172.

555 **FIGURE LEGENDS**

556 Fig. 1. Clinical pathologies of mice infected with SFTSV. Wild-type C57BL/6 (WT),
557 *Ifnar1*$^{-/-}$, *Stat*1$^{-/-}$, and *Stat*2$^{-/-}$ mice were infected with 10 FFU of SFTSV (YG1). (A)
558 Survival and (B) body weight changes were observed daily for 14 days pi (n = 10). For
559 WBC and PLT counts, blood samples were collected from two male and three female
560 mice at 0, 1, 3, 5, and 7 days pi. The values are shown as mean ± Standard Divisions
561 (SDs).

562

563 Fig. 2. Titers of SFTSV in mouse organs. Mice were inoculated with 10 FFU of SFTSV
564 YG1. Three female mice were euthanized for virus titration at 3, 5, and 7 days pi. The
565 virus titers in the mouse brains, lungs, livers, spleens, kidneys, intestines, and plasma
566 were measured by focus forming assay. The values are shown as mean ± SDs (n = 3).
567 *$P < 0.05$, compared among each mouse strain.

568

569 Fig. 3. The function of NSs as an IFN antagonist in human and murine cells. (A) HEK
570 293T or NIH3T3 cells transfected with the reporter plasmids were mock-infected or
571 infected with SFTSV. Two days after infection, cells were lysed to measure luciferase
572 activity and to examine the protein expression using immunoblotting. Relative light
573 units (RLU) in mock-infected cells were set as 1. Fold activation by SFTSV infection

574 are indicated. (B) The reporter plasmids were transfected into HEK293T or NIH3T3
575 cells with or without the expression plasmid for NSs. Twenty-four hours after
576 transfection, cells were treated with or without IFN-αA/D (500 U/ml) for 18 hours and
577 then were lysed to measure luciferase activity and detect protein expression using
578 immunoblotting. RLU in cells transfected with the empty vector or the indicated amount
579 of NSs expression plasmid in the absence of IFN-αA/D were set as 1. Fold activation by
580 IFN-αA/D are indicated. (C) The experiment done in (B) was repeated using the
581 expression plasmid for mMARV VP40 in NIH3T3 cells. (D) NSs expression plasmid (1
582 μg or 1.5 μg) or control plasmid was transfected into HEK293T or NIH3T3 cells,
583 respectively. Twenty-four hours after transfection, the cells were treated with IFN-αA/D
584 (200 U/ml) or left untreated for 10 hours. Expression levels of *Isg56* and *Oas1* mRNAs
585 in each cell line were measured by real-time qPCR. The mRNA expression levels of
586 ISG56 and OAS1 in IFN-αA/D untreated cells were set as 1. Fold activations by
587 IFN-αA/D are indicated. These assays were independently performed in triplicate. The
588 data represent averages with SDs. **in panel A and B, $P < 0.05$ versus no NSs.
589
590 Fig. 4. Interaction of NSs with STAT1 and STAT2. (A) HEK293T or NIH3T3 cells were
591 transfected with the expression plasmid for HA-tagged NSs and co-IP assays were

performed. (B) NIH3T3 cells were transfected with the expression plasmids for HA-tagged NSs and His-tagged hSTAT2 or hamSTAT2. The protein expression levels in cell lysates (left) and in co-IP assays (right) using an anti-HA or anti-His antibody. (C) Colocalization of NSs with STAT2. HEK293T, NIH3T3, or BHK-21 cells were transfected with the expression plasmid for HA-tagged NSs and the expression plasmid for His-tagged hSTAT2, mSTAT2, or hamSTAT2, respectively. IFA was also performed with NSs, STAT2, and the nuclei shown in green, red, and blue, respectively.

Fig. 5. Determination of the region of hSTAT2 important for the binding to NSs. (A) Schematic representation of the chimeric mutants of hSTAT2 and mSTAT2. (B) NIH3T3 cells were cotransfected with the expression plasmids for HA-tagged NSs and each of the STAT2 His-tagged chimeras. Representative results from the protein expression check in cell lysates (upper) and the co-IP assays using an anti-His antibody (lower) are shown. (C) IFA was also performed with NSs, STAT2, and the nuclei shown in green, red, and blue, respectively.

Fig. 6. Function of the NSs binding-deficient STAT2 chimera. The reporter plasmids were cotransfected into HEK293T cells with the expression plasmids for NSs and each

610 STAT2 chimera. Twenty-four hours after transfection, cells were treated with or without
611 IFN-αA/D (500 U/ml) for 18 hours and then were lysed to measure luciferase activity
612 (upper figure) or detect protein expression using immunoblotting (lower figure). The
613 ISRE activity was calculated by dividing RLU in IFN-αA/D-treated cells by the units
614 IFN-αA/D untreated cells. The ISRE activity in the absence of NSs was set as 100%.
615 The assays were independently performed in triplicate. The data represent averages with
616 SDs. ** $P < 0.05$ versus hSTAT2.
617
618 Fig. 7. Suppression of STAT2 phosphorylation by NSs. (A) HEK293T or NIH3T3 cells
619 transfected with the expression plasmid for HA-tagged NSs were treated with
620 IFN-αA/D (2000 U/ml) or left untreated for 45 minutes and were then lysed for
621 detection of each protein expression by immunoblotting. (B) HEK293T or NIH3T3 cells
622 infected with SFTSV at an MOI of 10 were treated with IFN-αA/D (2000 U/ml) or left
623 untreated for 45 minutes and were then lysed for detection of each protein expression by
624 immunoblotting.
625

Table 1. List of the primers used in this study

Primer name	Primer sequence	Remarkes
pcDNA-NSsHA-RV-F	atccaccatgtcgctgagcaaatgctccaac	For the construction of pcDNA3.1/NSs-HA
pcDNA-NSsHA-Kpn-R	gcttggtacctcaagcgtaatctggaacatcgtat ggatagacctccttcgggaggtcacc	
humanSTAT2hisF	atccaccatggcgcagtgggaaatgctg	For the construction of pcDNA3.1/hSTAT2-His
humanSTAT2hisR	gcttggtacctcaatggtgatggtgatgatgaccg gtatgcatattgaagtcagaaggcatcaagggtcc	
mouseSTAT2hisF	atccaccatggcgcagtgggagatgttg	For the construction of pcDNA3.1/mSTAT2-His
mouseSTAT2hisR	gcttggtacctcaatggtgatggtgatgatgaccg gtatgcatattgaaggtatcaagagtccatcccaa	
hamSTAT2F	atccaccatggcgcagtgggagacactg	For the construction of pcDNA3.1/hamSTAT2-His
hamSTAT2hisR	gcttggtacctcaatggtgatggtgatgatgaccg gtatgcatattgtcatcagaaggaatcaagggtcc	
mSTAT2-hDBD-veF	gttcttctgccaagctccgaaag	For the construction of pHHM(#1)
HMM-HHM-inR	accggtatgcatattgaaggtatc	
hmSTAT2DBDveF	aatatgcataccggtcatcatcac	
mSTAT2-hDBD-inR	gcttggcagaagaactgctggttctgaagg	
hSTAT2-mDBD-inF	acagagcctttgtagtagaaacccagccctg	For the construction of pHMM(#2)
HMM-HHM-inR	accggtatgcatattgaaggtatc	
hmSTAT2DBDveF	aatatgcataccggtcatcatcac	
hSTAT2-mDBD-veR	ctacaaaggctctgtggagcag	
mSTAT2-hDBD-inF	aaaggtcctttgtggtagaaacccagccc	For the construction of pMHH(#3)
MMH-MHH-inR	accggtatgcatattgaagtcag	
hmSTAT2DBDveF	aatatgcataccggtcatcatcac	
mSTAT2-hDBD-veR	ccacaaaggacctttggagcagac	
hSTAT2-mDBD-veF	gttcttctccaacccccccaag	For the construction of pMMH(#4)
MMH-MHH-inR	accggtatgcatattgaagtcag	
hmSTAT2DBDveF	aatatgcataccggtcatcatcac	
hSTAT2-mDBD-inR	gggttggagaagaactgctggttcttggg	
H(1-100)MMinF	cccaggatcctacccagttggctgagatg	For the construction of pH(1-100)MM(#5)
HMM-HHM-inR	accggtatgcatattgaaggtatc	
hmSTAT2DBDveF	aatatgcataccggtcatcatcac	
H(1-100)MMVeR	gggtaggatcctgggaaaagggctgaatg	
H(1-221)MMinF	cactgctaggccgattaaccaccctgg	For the construction of pH(1-221)MM(#6)
HMM-HHM-inR	accggtatgcatattgaaggtatc	
hmSTAT2DBDveF	aatatgcataccggtcatcatcac	
H(1-221)MMVeR	atcggcctagcagtgctttggaggcatc	

Table 1. (Continued)

Primer name	Primer sequence	Remarkes
H222-315inF	gactggttggccgattaactaccctaatcg	
hSTAT2-mDBD-veR	ctacaaaggctctgtggagcag	For the construction of
hSTAT2-mDBD-inF	acagagcctttgtagtagaaacccagccctg	pH(222-315)MM(#7)
H222-315veR	atcggccaaccagtccttggagatgtcc	
MH(101-315)MMinF	cccaatggccctacccagttggctgagatg	
hSTAT2-mDBD-veR	ctacaaaggctctgtggagcag	For the construction of
hSTAT2-mDBD-inF	acagagcctttgtagtagaaacccagccctg	pH(101-315)MM(#8)
MH(101-315)MMveR	ggtagggccattgggaaaggtctgaatatc	
MH(101-315)MMinF	cccaatggccctacccagttggctgagatg	
HMM-HHM-inR	accggtatgcatattgaaggtatc	For the construction of
hmSTAT2DBDveF	aatatgcataccggtcatcatcac	pH(101-315)HM(#9)
MH(101-315)MMveR	ggtagggccattgggaaaggtctgaatatc	
MARV VP40 S15PF	cttgaacccccctccttatgctgatcacgg	
MARV VP40 S15PR	tattgcatgtatgtgttgtaattgctggaactggcc	For the construction of
MARV VP40 G79SF	gttccggcatggctgcctcttgg	pmMARV VP40
MARV VP40 G79SR	gcttttgactgttcgctcgttatatgcagatatgtc	
hISG56F	cctccttgggttcgtctaca	For the Real-time RT-PCR
hISG56R	ggctgatatctgggtgccta	detection of human ISG56 (Ref: 13)
mISG56F	accatgggagagaatgctgat	For the Real-time RT-PCR
mISG56R	gccaggaggttgtgc	detection of mouse ISG56 (Ref: 30)
hOAS1realF	catccgcctagtcaagcactg	For the Real-time RT-PCR
hOAS1realR	caccacccaagtttcctgtag	detection of human OAS1 (Ref: 13)
mOAS1realF	gcctggtcacgcactggta	For the Real-time RT-PCR
mOAS1realR	aagccctgggctgtgttg	detection of mouse OAS1 (Ref: 31)
hGAPDH-F	atggggaaggtgaaggtcgg	For the Real-time RT-PCR
hGAPDH-R	ttactccttggaggccatgtg	detection of human GAPDH
mGAPDH-F	aggtcggtgtgaacggatttg	For the Real-time RT-PCR
mGAPDH-R	tgtagaccatgtagttgaggtca	detection of mouse GAPDH (Ref: 32)

628

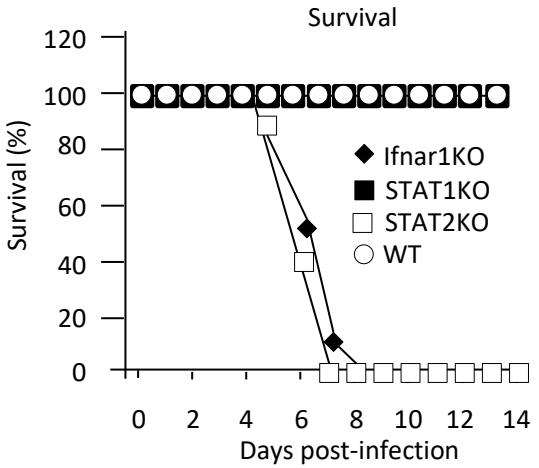
Survival
Survival (%)
120
100
80
60
40
20
0
Ifnar1KO
STAT1KO
STAT2KO
WT
0 2 4 6 8 10 12 14
Days post-infection

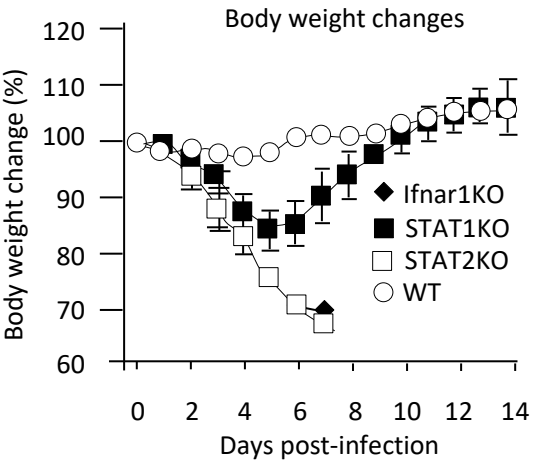
Body weight changes
Body weight change (%)
120
110
100
90
80
70
60
Ifnar1KO
STAT1KO
STAT2KO
WT
0 2 4 6 8 10 12 14
Days post-infection

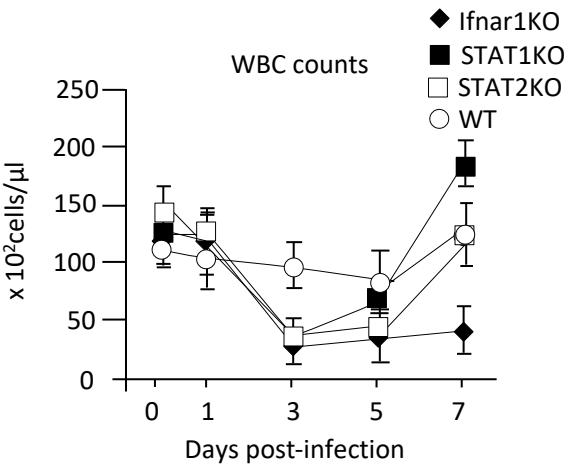
WBC counts
x 10²cells/µl
250
200
150
100
50
0
Ifnar1KO
STAT1KO
STAT2KO
WT
0 1 3 5 7
Days post-infection

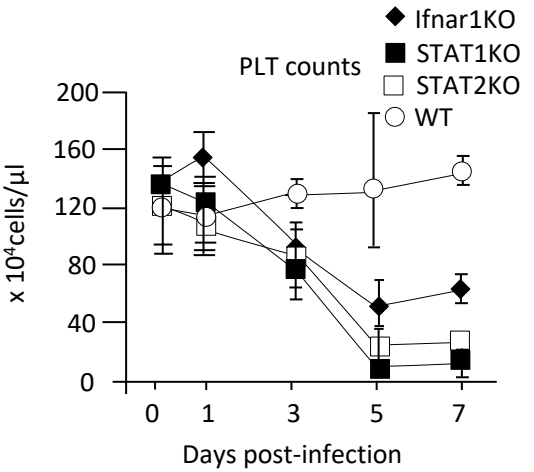
PLT counts
x 10⁴cells/µl
200
160
120
80
40
0
Ifnar1KO
STAT1KO
STAT2KO
WT
0 1 3 5 7
Days post-infection

Fig.1

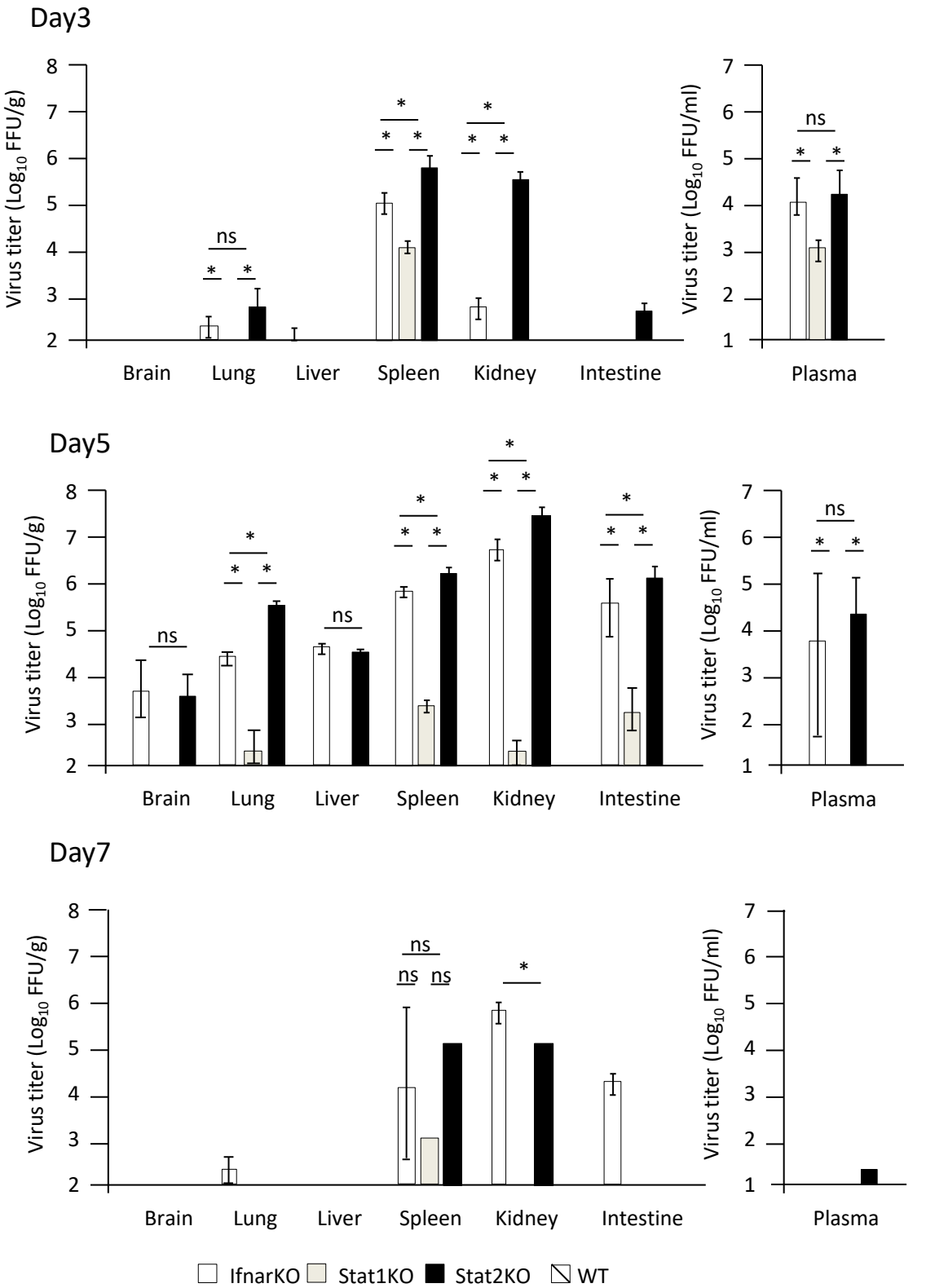
Day3
Virus titer (Log10 FFU/g)
Virus titer (Log10 FFU/ml)
ns
Brain
Lung
Liver
Spleen
Kidney
Intestine
Plasma
Day5
Day7
IfnarKO
Stat1KO
Stat2KO
WT

Fig.2

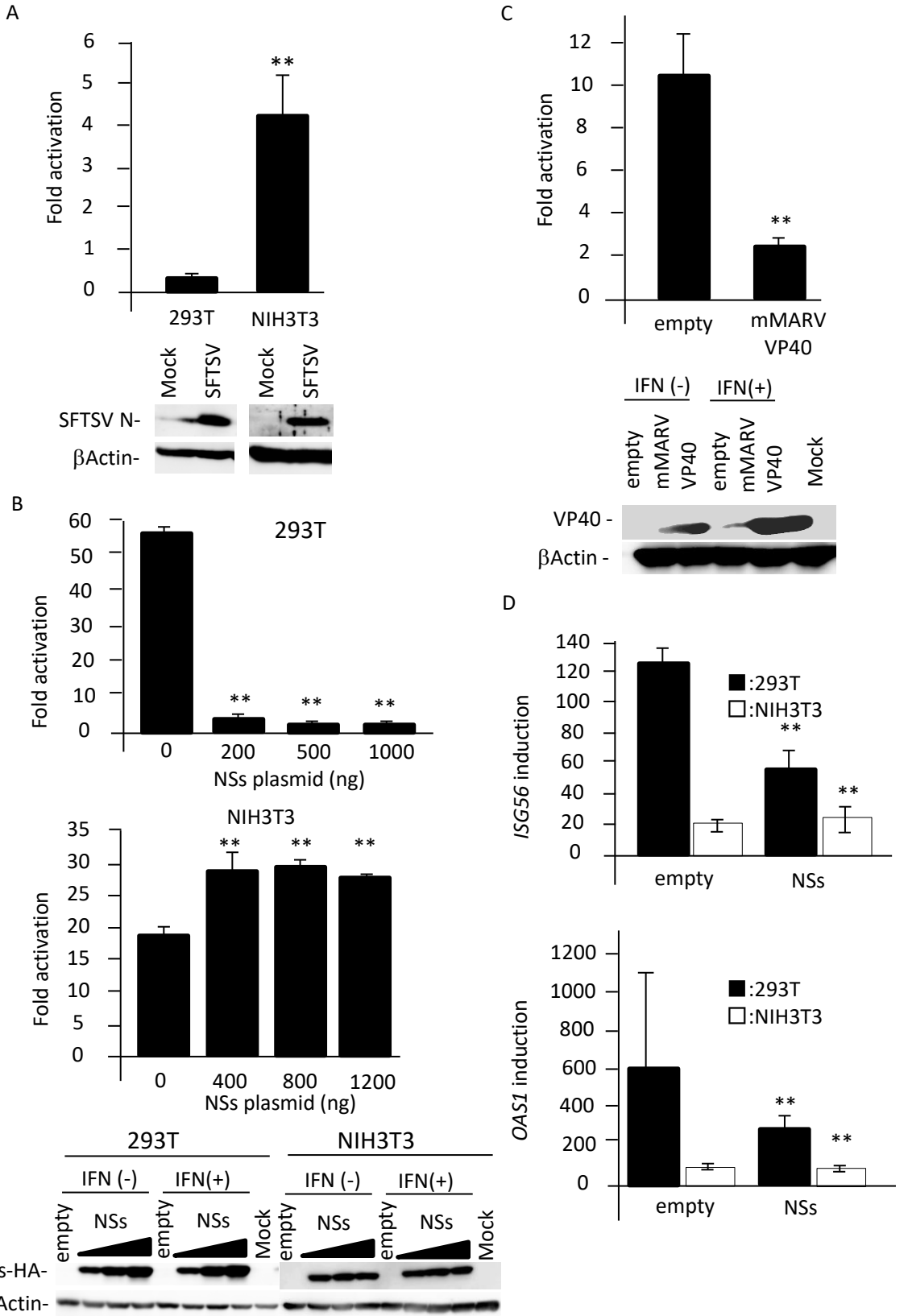
A
Fold activation
293T
NIH3T3
Mock
SFTSV
SFTSV N-
βActin-
B
293T
Fold activation
NSs plasmid (ng)
NIH3T3
293T
NIH3T3
IFN (-)
IFN(+)
empty
NSs
Mock
NSs-HA-
βActin-
C
Fold activation
empty
mMARV VP40
IFN (-)
IFN(+)
VP40 -
βActin -
D
ISG56 induction
:293T
:NIH3T3
OAS1 induction
empty
NSs

Fig.3

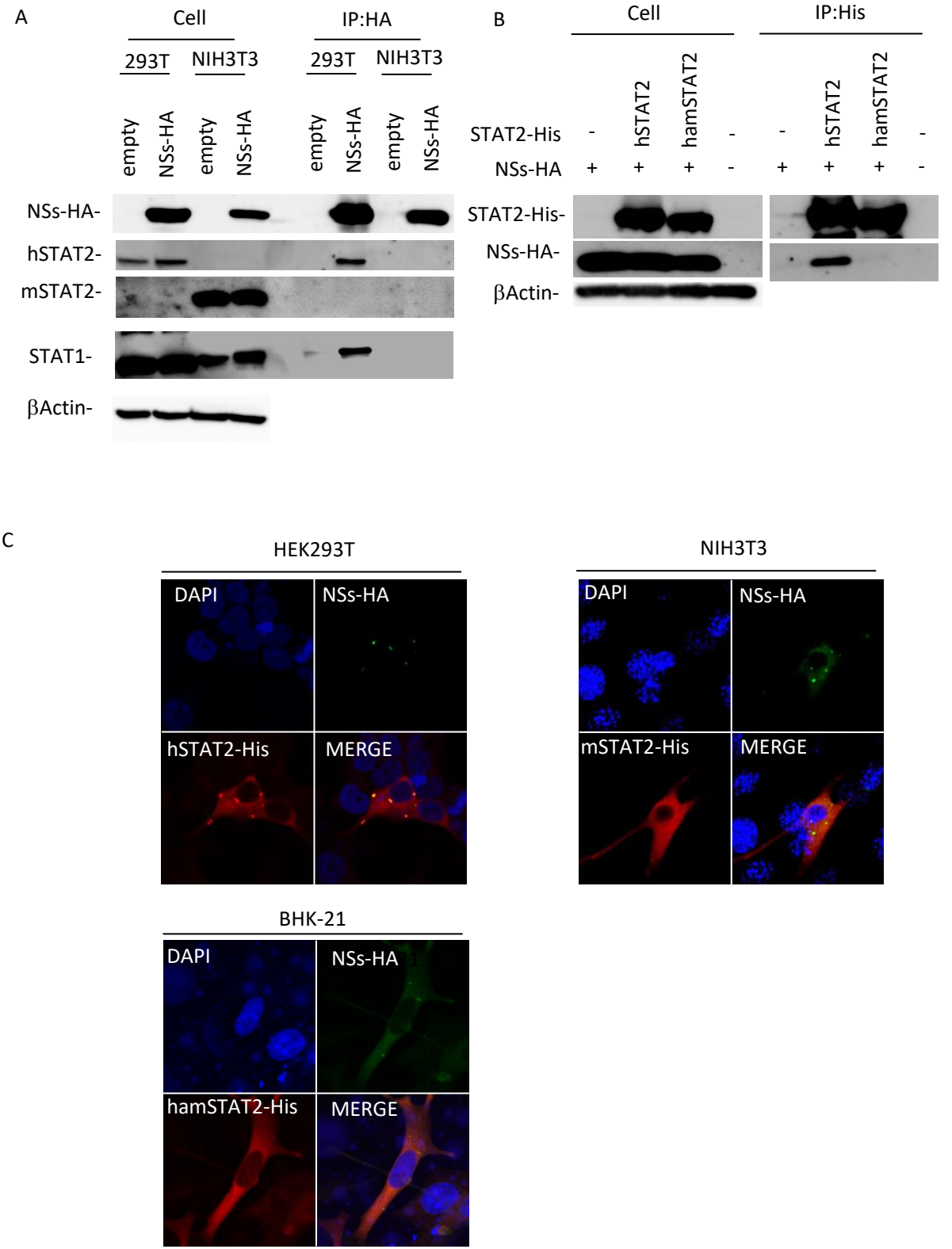
A
Cell
IP:HA
293T
NIH3T3
293T
NIH3T3
empty
NSs-HA
empty
NSs-HA
empty
NSs-HA
empty
NSs-HA
NSs-HA-
hSTAT2-
mSTAT2-
STAT1-
βActin-
B
Cell
IP:His
STAT2-His
NSs-HA
hSTAT2
hamSTAT2
STAT2-His-
NSs-HA-
βActin-
C
HEK293T
DAPI
NSs-HA
hSTAT2-His
MERGE
NIH3T3
DAPI
NSs-HA
mSTAT2-His
MERGE
BHK-21
DAPI
NSs-HA
hamSTAT2-His
MERGE

Fig.4

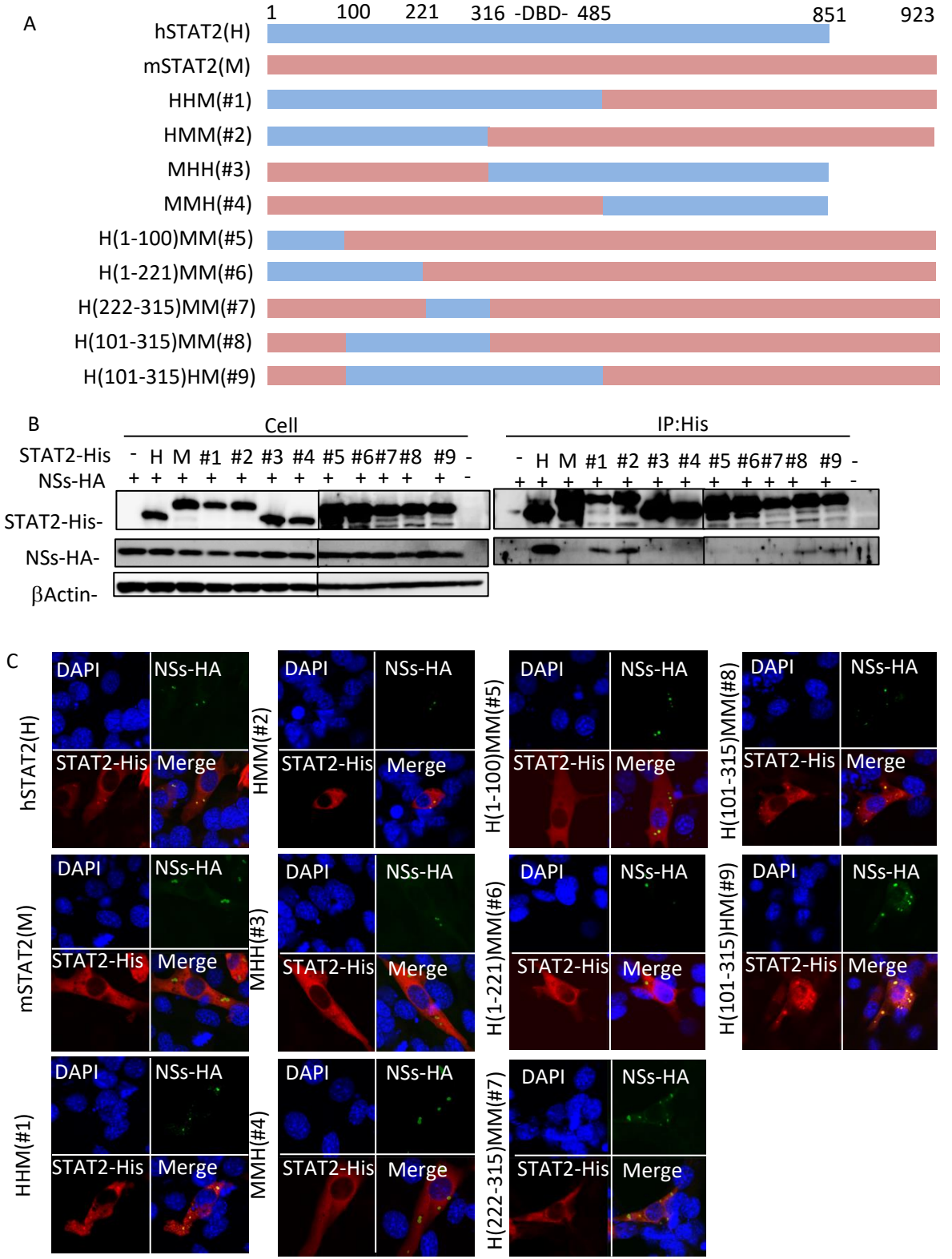
A
1
100
221
316
-DBD-
485
851
923
hSTAT2(H)
mSTAT2(M)
HHM(#1)
HMM(#2)
MHH(#3)
MMH(#4)
H(1-100)MM(#5)
H(1-221)MM(#6)
H(222-315)MM(#7)
H(101-315)MM(#8)
H(101-315)HM(#9)
B
Cell
IP:His
STAT2-His
NSs-HA
STAT2-His-
NSs-HA-
βActin-
C
DAPI
NSs-HA
STAT2-His
Merge

Fig.5

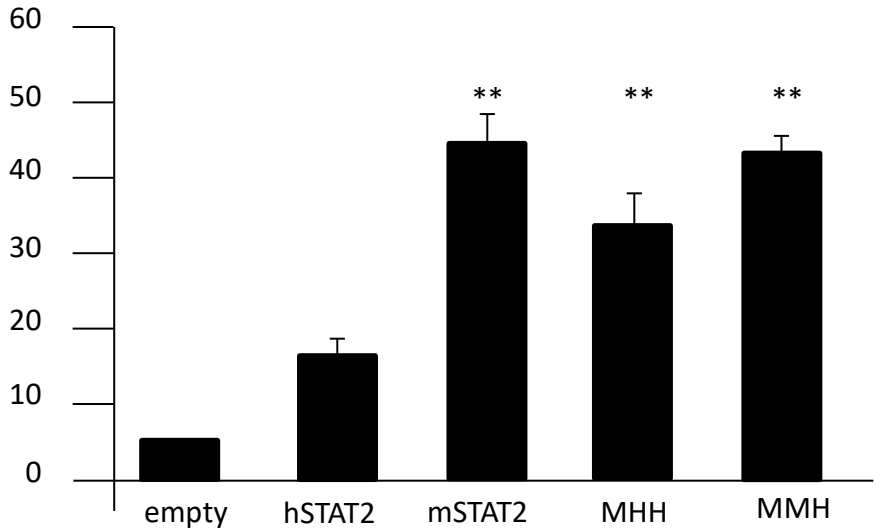
60
50
40
30
20
10
0
**
**
**
empty
hSTAT2
mSTAT2
MHH
MMH

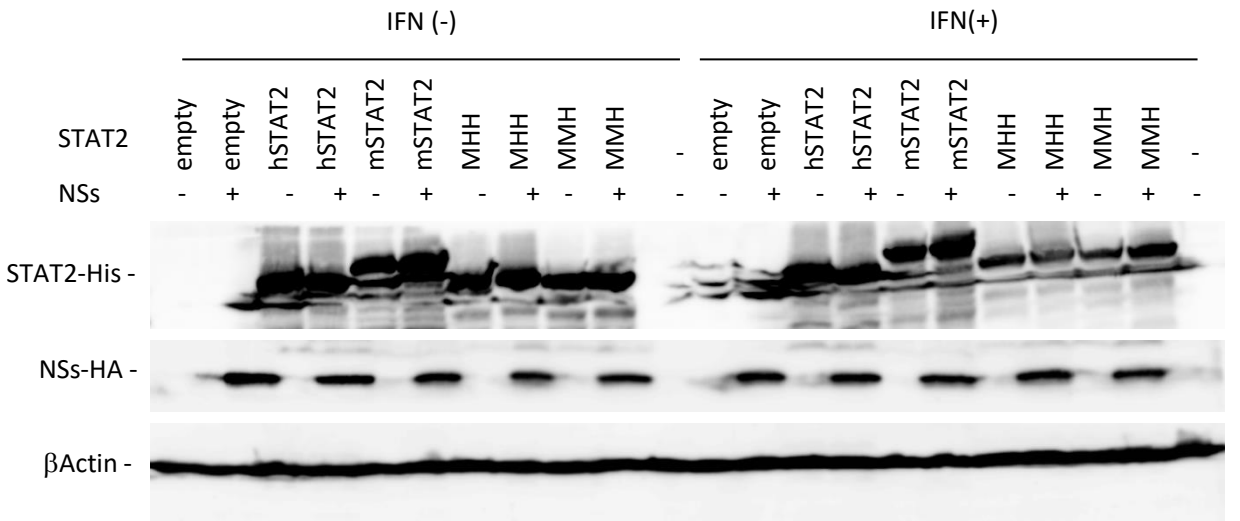
IFN (-)
IFN(+)
STAT2
NSs
empty
empty
hSTAT2
hSTAT2
mSTAT2
mSTAT2
MHH
MHH
MMH
MMH
-
STAT2-His -
NSs-HA -
βActin -

Fig.6

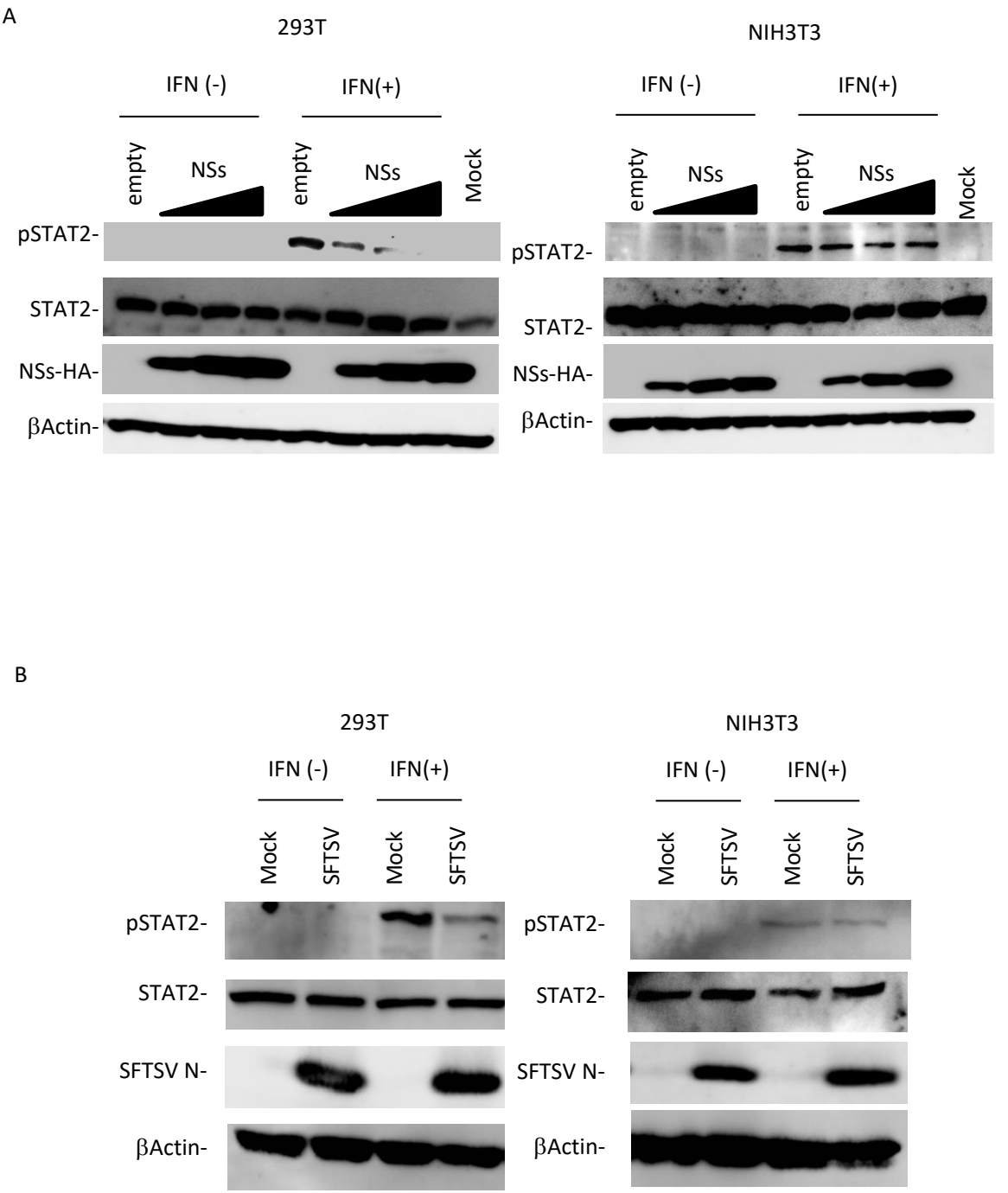
A
293T
NIH3T3
IFN (-)
IFN(+)
empty
NSs
Mock
pSTAT2-
STAT2-
NSs-HA-
βActin-
B
293T
NIH3T3
IFN (-)
IFN(+)
Mock
SFTSV
pSTAT2-
STAT2-
SFTSV N-
βActin-

Fig.7